INL/CON-23-71863-Revision-1

Numerical study of proppant transport and settling processes in fractures

October 2023

Changing the World's Energy Future

Robert Egert, Wencheng Jin, Chunfang Meng, Aim Fournier

Idaho National Laboratory

INL/CON-23-71863-Revision-1

Numerical study of proppant transport and settling processes in fractures

Robert Egert, Wencheng Jin, Chunfang Meng, Aim Fournier

October 2023

Idaho National Laboratory
Idaho Falls, Idaho 83415

http://www.inl.gov

Prepared for the
U.S. Department of Energy
Under DOE Idaho Operations Office
Contract DE-AC07-05ID14517

GRC Transactions, Vol. 47, 2023

Numerical Study of Proppant Transport and Settling Processes in Fractures

Robert Egert[1], Chunfang Meng[2], Aimé Fournier[3] and Wencheng Jin[1]

[1]Energy and Environment Science and Technology Directorate, Idaho National Laboratory, USA

[2]Eden Geopower, Somerville, Massachusetts, USA

[3]Earth Resources Laboratory MIT, Cambridge, Massachusetts, USA

Keywords

Hydraulic fracturing, Fracture flow, Proppant transport, Slurry

ABSTRACT

Reservoir stimulation by creating hydraulically conductive fractures is the key step for enabling enhanced geothermal systems (EGS). The effectiveness of stimulation is significantly influenced by the deposition of proppant inside induced fractures. The transportation and settling of proppant in a propagating fracture is controlled by a multitude of operational and physical parameters, including the fracturing fluid rheology, injection rate, proppant concentration, fracture length/aperture evolution, proppant size/density/shape, etc. A numerical tool that robustly and efficiently accounts for all important attributes can facilitate the design and optimization of reservoir stimulation. This study presents the novel computational tool ELK (ELectrical fracKing) developed for the numerical simulation of proppant-fluid mixture circulation in a fractured geothermal reservoir. We enriched the MOOSE-based PorousFlow module with a suite of equations to consider the fluid-proppant mixture with particle-particle/fluid interactions, which include gravitational settling, particle convection, particle hampering, and strong density and viscosity contrasts. The computational tool is validated by comparing the predicted proppant bed evolution against two different laboratory scale experiments of proppant transport in a fixed aperture channel. Further parameter studies were performed, and the modeling results show that the proppant deposition is determined by the mixing characteristics and settling of the particles from the slurry. Concentration-dependent density and viscosity lead to an inhomogeneous distribution of the proppant, particle collision, and enhanced settling at the bottom of the fractures. Preliminary coupling with dynamic fracture propagation shows promising results and will be further developed to simulate hydraulic stimulation at high fidelity.

1. Introduction

Hydraulic fracturing is a technique for creating or enhancing fractures and fracture networks in tight formations to increase the permeability of reservoirs. The technique has been applied to various kinds of geoscientific reservoirs, like unconventional oil or gas reservoirs (Adachi et al., 2007), as well as enhanced geothermal systems (Schill et al., 2017). Hydraulic fracturing is a coupled multistage process involving rock deformation, crack propagation, and fluid flow therein (Barboza et al., 2021). A large volume of water is injected under high pressure through a wellbore into a reservoir to create a fracture in the reservoir and/or enlarge it. However, as soon as the fluid pressure is released, the opened crack closes again due to in situ stress, causing the hydraulic pathways created to be lost (Adachi et al., 2007). To avoid this effect, small sand or graphite particles called proppants are added to the fracturing fluid, which are carried into the fracture and prevent it from closing. The mixture of proppant particles and fracturing fluid is called slurry. The proppant particles remain in the fracture and keep it open with at least the particle size, while the fracturing fluid is retrieved from the wellbore. Therefore the transport and distribution of the proppant within the fracture are of critical importance for the success of the hydraulic treatment (Kumar et al., 2019). The final distribution of proppants in the stimulated fracture is highly affected by the injection strategy and the material properties of the injected proppant and fracturing fluid (Hu et al., 2018). High density contrasts between the fluid and the solid proppant particles could cause early settling and jamming of the fracture, preventing it from propagating further into the reservoir (Kumar et al., 2019). Many experimental studies of proppant dispersion and settling at laboratory and field scales can be found in the literature, providing a good basis for formulating empirical correlations and validating numerical models (Isah et al., 2021).

Numerical modeling is an indispensable tool for understanding reservoirs' relevant processes and underlying physics during operation and/or hydraulic stimulation (Egert et al., 2020). In principle, the processes of proppant transport during stimulation can be treated as multiphase flow simulations of two interpenetrating media (Barboza et al., 2021). Two groups of approaches are adopted in literature and differ in the treatment of the dispersed phase: Eulerian-Eulerian and Eulerian-Lagrangian schemes (Barboza et al., 2021; Wang and Elsworth, 2018). In the Eulerian-Lagrangian scheme, the fluid is a continuum and proppant particles are simulated as shape-dissolved particles. Numerical models describe the forces acting on and in between each particle, particle-wall interactions and the solution is given in time, location, and velocity. The approach is advantageous to capture the underlying physics and for multi-sized proppants, but it suffer from being computationally expensive and it’s limited applicability to field-scale (Huang et al., 2022). Eulerian-Eulerian scheme treats both, the fracturing fluid and proppant, as continua governed by the mass conservation (Shiozawa and McClure, 2016). The particle phase can interact with the fluid. The slurry transport is modeled either as a two-phase flow or as a mixture flow with a concentration-dependent fluid rheology (Adachi et al., 2007; Barree and Conway, 1995; Kumar et al., 2019). Advantage of the Eulerian-Eulerian scheme is computational efficiency, whereas physical processes like particle-particle interactions and the resulting relative motion rely on empirical correlations derived from experiments (Huang et al., 2022).

The model proposed in this study follows the Eulerian-Eulerian scheme and simulates the transport of proppant particles in a carrying fluid assuming a slurry mixture. Several mechanisms like particle settling, particle-particle interactions, jamming and proppant bed formation are considered. The fluid flow within the fracture is governed by a mass conservation equation of the slurry with density and viscosity depending on the volumetric proppant concentration. Once the settled proppant reaches maximum saturation, it forms an immobile bed, and the fluid properties only consider the fracturing fluid. The velocity of the proppant is related to the fluid velocity by means of a slip velocity that takes into account all the aforementioned effects, supported by different empirical correlations.

In the presented study, we focus on calibrating and validating the developed proppant transport workflow. Therefore, we compare the results of numerical simulations with results gained from two different laboratory experiments. In these experiments, a slurry made of high-density proppant and low-viscosity water is injected into a 2D vertical, parallel-walled fracture of constant aperture. Based on the calibrated workflow, numerical simulations are conducted to identify and evaluate the critical parameters for proppant transport using different kinds of fluid (e.g., slickwater, gel). The model is extended to account for an impermeable 3D host rock and to include spatially and temporally varying fracture apertures resulting from KGD fracture propagation. Upscaling the newly developed workflow will allow us to evaluate and optimize the hydraulic fracturing treatment for different field-scale applications.

2. Material & methods

The numerical simulations are carried out with a finite element (FE) application called ELK (ELectrical fracKing). The code is based on the open-source MOOSE (Multiphysics Object-Oriented Simulation Environment) framework (Lindsay et al., 2022) and utilizes the PorousFlow and TensorMechanics modules (Wilkins et al., 2021) for a fully coupled solution of thermo-hydro-mechanical processes in a fractured and porous medium. These equations were extended to include the mixture at various proppant concentrations and its associated specific flow equations. The code allows for flexible and multidimensional analysis and solution of physical processes considering 3D lithologic units as well as lower dimensions such as 2D fractures and 1D wells.

2.1 Slurry flow

In the developed workflow, the fracturing fluid and the proppant particles are treated as a single-phase mixture and solved as continua of interpenetration, where a volume cell can be occupied simultaneously by a mixture of both components. Therefore, the volume fraction is introduced to indicate how much space is occupied by each component at a given time. The mutual coupling between the particles and the fluid must be taken into account, since the particles will move along with the fluid. The proppant settling and gravitational segregation out of the slurry is controlled by the properties of the proppant particles and the carrying fluid, causing strong variations in the mixture density and viscosity and the formation of an immobile bedding at the bottom of a fracture (Huang et al., 2022).

The following mass balance and constitutive equations are used to solve the proppant - carrying fluid mixture as an incompressible slurry flow

$$\frac{\partial}{\partial t}(\rho_m) + \nabla . (\rho_m \boldsymbol{v_m}) = 0 \tag{1}$$

where ρ_{m} is the slurry (mixture) density and $\boldsymbol{v_m}$ is the darcy velocity vector of the slurry as

$$\boldsymbol{v_m} = -\frac{k_f}{\mu_m}(\nabla \mathrm{p} - \rho_m \boldsymbol{g}) \tag{2}$$

where μ_m is the viscosity of the slurry, and $\mathbf{g}$ is the gravity vector. The fracture permeability component in the direction parallel to the fracture k_f, which is dependent on the fracture aperture a via

$$\boldsymbol{k_f} = \frac{a^2}{12} \tag{3}$$

The mass conservation for the proppant in a lower-dimensional fracture can be obtained using Eq. 4 as

$$\frac{\partial}{\partial t}(c\,a) + \nabla\cdot\left(c\,a\,\boldsymbol{v_p}\right) = 0 \tag{4}$$

where c and $\boldsymbol{v}_\mathrm{p}$ denote the proppant volume fraction and velocity, respectively. For the governing equations, the relationships for the bulk density and velocity vector between slurry, fluid and proppant can be expressed as follows

$$\rho_m = (1 - c)\,\rho_f + \mathrm{c}\,\rho_p \tag{5}$$

$$\rho_m \boldsymbol{v_m} = (1 - c)\,\rho_f\,\boldsymbol{v_f} + \mathrm{c}\,\rho_p\,\boldsymbol{v_p} \tag{6}$$

where ρ_f and $\boldsymbol{v}_\mathrm{f}$ denote the carrying fluid density and velocity, ρ_p is the proppant particle density.

The governing equations for fluid, proppant, and slurry are complementary to each other, so only two equations need to be solved. In addition, different constitutive models are needed to close the system of equations. The proppant particle velocity $\boldsymbol{v_p}$ is related to the carrying fluid velocity by the slip velocity $\boldsymbol{v_{slip}}$

$$\boldsymbol{v_{slip}} = \boldsymbol{v_p} - \boldsymbol{v_f} \tag{7}$$

and can be expressed as a function of the slurry velocity

$$\boldsymbol{v_p} = \boldsymbol{v_m} + (\boldsymbol{1} - \boldsymbol{c})\,\boldsymbol{v_{slip}} \tag{8}$$

The slip velocity $\boldsymbol{v}_\mathrm{slip}$ considers vertical gravitational particle settling as well as horizontal collisional effects and fluid-particle drag forces. The gravitational component $\boldsymbol{v_{slip,V}}$ can be expressed as

$$\boldsymbol{v_{slip,V}} = \boldsymbol{f}(\boldsymbol{c})\,\boldsymbol{v_{stokes}} \tag{9}$$

where $\boldsymbol{v}_\mathrm{stokes}$ is the settling velocity of a single proppant particle in an infinitely large space obtained from the Stokes drag law. The equation is valid for low Reynolds number (Re < 2) and expressed as

$$\boldsymbol{v_{stokes}} = \left(\rho_p - \rho_f\right)\frac{g\,d_p^2}{18\,\mu_f} \tag{10}$$

Where μ_f is the fluid viscosity and $\mathrm{d_p}$ is the proppant particle diameter. For intermediate and high Reynolds numbers (Re > 2 and Re > 500) the single particle settling velocity is derived experimentally and expressed as (Barboza et al., 2021; Barree and Conway, 1995)

$$\boldsymbol{v_{stokes}} = 0.2\, d_p^{1.18} \left[\frac{g\,(\rho_p - \rho_f)}{\rho_f}\right]^{0.71} \left(\frac{\rho_f}{\mu_f}\right)^{0.45} \tag{11}$$

$$\boldsymbol{v_{stokes}} = 1.74\, d_p^{0.5} \left[\frac{g\,(\rho_p - \rho_f)}{\rho_f}\right]^{0.5} \tag{12}$$

The correction factor f(c) takes into account the effect of hindered settling due to particle-particle interactions and is derived experimentally. Barree and Conway (1995) proposed an empirical model for f(c) as follows

$$\boldsymbol{f(c)} = e^{-\lambda_s c} \tag{13}$$

with λ_s as the hindered settling coefficient, typically between 4 and 6. Further models proposed are e.g., by Gadde et al. (2004) and Clark and Quadir (1981). The horizontal component of slip velocity $\boldsymbol{v}_{\mathrm{slip,H}}$ is often neglected, and slurry and particle velocities are considered equal (Adachi et al., 2007; Hu et al., 2018). Barree and Conway (1995) proposed a formulation, which considers the collisional effects between the particles in the horizontal slip velocity proposed as

$$\boldsymbol{v_{slip,H}} = \frac{\lambda - 1}{1 - c}\, v_m^{vol} \tag{14}$$

where v_m^{vol} is the volume average horizontal slurry velocity. λ is a correction factor to account for the greatest particle slip c_{slip} and the empirical constants α and β

$$\lambda = \left[\alpha - \left|c - c_{slip}\right|^{\beta}\right] \tag{15}$$

These factors are determined empirically and usually assumed to be $\alpha = 1.27$, $\beta = 1.5$ and $c_{slip} = 0.1$, but can be varied throughout the simulations (Barree and Conway, 1995). This empirical model takes into account a reduction in horizontal particle velocity close to maximum proppant concentration c_{max}.

The viscosity of the slurry μ_m is a function of the volumetric proppant concentration. While there exist a numerous of empirical model in literature, this implementation focusses on the exponential equation based on Nicodemo et al. (1974) to describe the bulk apparent viscosity as

$$\mu_m = \mu_f \left[1 + 1.25 \left(\frac{c}{1 - \frac{c}{c_{max}}}\right)\right]^2 \tag{16}$$

where μ_m is the slurry viscosity and μ_f is the Newtonian effective viscosity of the fracturing fluid. Further models were proposed e.g. by Adachi et al. (2007) or Shook and Roco (1991). In order to avoid division by zero and infinite viscosity, c is limited in our simulations to 0.9 c_{max}. Since the finite element method for flow-related problems is conditionally unstable, an upwinding scheme is introduced into the model to limit the onset of spurious oscillations (Wilkins et al., 2021). All presented equations are solved in a fully-coupled manner treating the fractions of carrying fluid and proppant as nonlinear variables sharing a common slurry flow equation (single-phase flow). Slurry flow properties (e.g., density and viscosity) as well as concentration-dependent settling properties are updated within each iteration. The change in flow regime is evaluated after each solved time step.

2.2 Proppant Bed Build-Up and Flow

In addition to the flow as a slurry, the proppant particles settle out of the suspension into an immobile bed at the bottom of a fracture until the maximum proppant packing is reached. Once saturation (i.e., maximum proppant concentration) is reached, the proppant behaves like a porous solid. The fluid can still mobilize and flow through the pores of the settled proppant pack. In order to account for these changes, the cubic law is no longer valid and flow in porous media is used instead, e.g., by considering the Kozeny-Carman relationship for particle size dependent porosity/permeability (Carman, 1937). The fluid rheology in the proppant bed is modified to account only for the density and viscosity of the fracturing fluid (Huang et al., 2022).

3. Results and discussion

3.1 Single inlet velocity injection

We validate our developed workflow with two different examples of experimental data and numerical codes. In the first step, our approach is compared against the experimental results of Tong and Mohanty (2016) and the subsequently developed model of Hu et al. (2018). In the experimental setup, a proppant slurry with a fixed concentration (c = 0.038) is injected in a vertical fracture with a constant injection velocity v_{inj} = 0.1 m.s^{-1} at the upper right corner (Figure 1). The pressure is maintained constant (p = 0.1 MPa) through an outlet at the upper left boundary of the vertical fracture. The proppant settles out of the slurry resulting a dune, which increases with injection time. The effect of the slurry leak-off is not considered because the experiment has no exit. The model and experimental setup are shown in Table 1.

Table 1: Properties for the first benchmark after Tong and Mohanty (2016)

Parameter	**Unit**	**Value**
Fracture width	m	0.002
Fracture length	m	0.381
Fracture height	m	0.0762
Proppant diameter	m	0.0006
Proppant density	kg.m^{-3}	2650
Saturation concentration	-	0.63
Inlet proppant concentration	-	0.038
Inlet slurry velocity	m.s^{-1}	0.1
Carrying fluid density	kg.m^{-3}	1000
Carrying fluid viscosity	Pa.s	0.001
Outlet pressure	Pa	100000

Figure 1 shows the simulated proppant concentration in the vertical fracture after t = 20, 40 and 60 s of continuous injection. Due to the low viscosity of the fluid, the injected proppant immediately settles out of the slurry. The proppant forms a dune with maximum saturation concentration at the bottom of the fracture, and the dune builds up from the right side of the fracture (dark red color). To compare the results between the different modeling and the experiments, the predicted and measured dune lengths and heights are compared at different time steps and with respect to the fracture height/length, following Hu et al. (2018). The dimensionless proppant bed height (DPDH) is defined as the height of the proppant bed at equilibrium over to the total fracture height shown in Figure 1. It depends on the settling rate compared to the advective velocity of the slurry. The dimensionless middle proppant transport length (DMPDL) describes the dune length, at the proppant bed height that equals 50% of the maximum bed height, over to the total fracture length. Figure 2 compares DPDH and DMPDL among different codes prediction against the experimental measurements. The average error between our simulations and the experiment results is 2.3 % for the DMPDL and 1.7 % for DPDH, respectively. Furthermore, the results for DPDH correspond to the analytical solution of the bi-power law model of Wang et al. (2003) with an average error of 1.5 %.

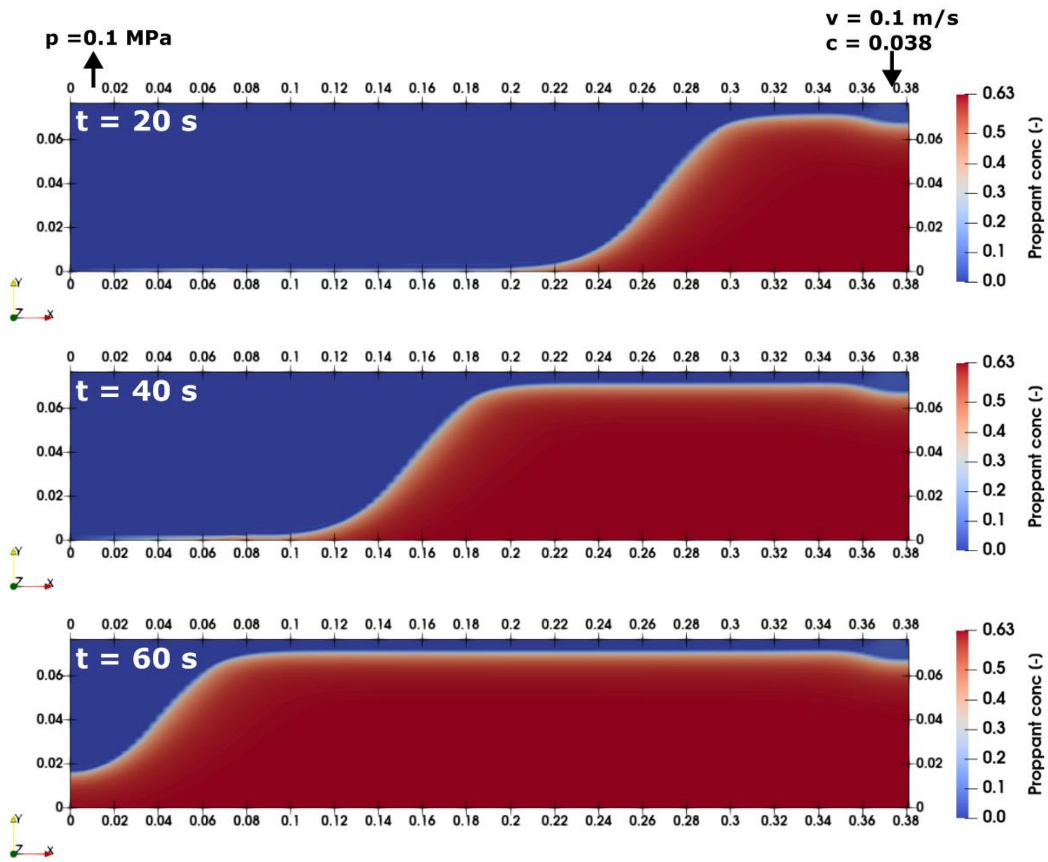

Figure 1: Proppant concentration in a vertical fracture with ongoing injection time. The slurry is injected on the upper right of the fracture.

Most differences of the result from the initial stage of the experiments are at regions where the proppant height is not in equilibrium yet and a steady flow regime is not established. But for the field application, results at far larger time scales are more important and our results tend to be in good agreement. Nevertheless, it is worth mentioning that our model even can reproduce the lowered proppant height opposite the inlet due to a zone of high advection velocity.

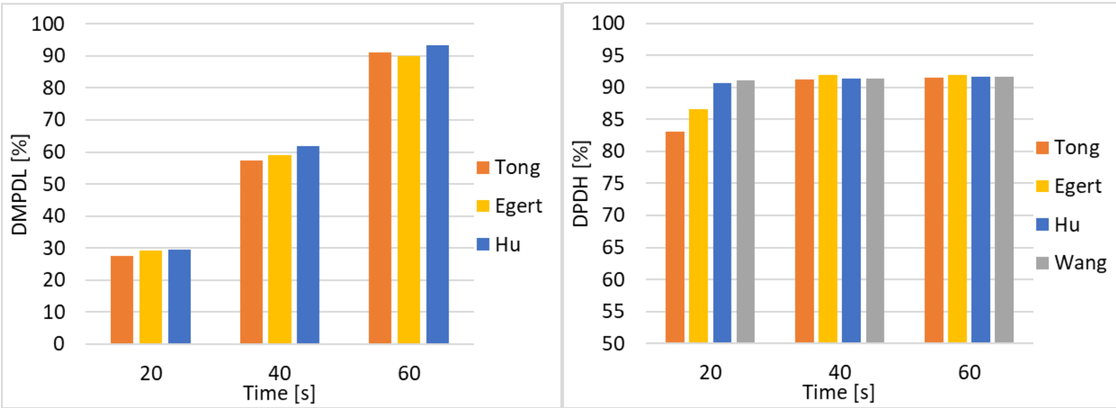

Figure 2: Comparison of our simulations results against the experimental results of Tong and Mohanty (2016) and numerical models of Hu et al. (2018)

3.2 Multi inlet injection

In the second example, our workflow is compared against a slot experiment performed by Chun et al. (2020) and simulated by Huang et al. (2022). In this experiment, slickwater was injected into a single inclined fracture through three individual inlets. The fracture was constrained by Plexiglas mimicking a non-permeable rock matrix. The dimensions of the fracture are 4 x 1 ft with a constant aperture of 0.3 in. The three inlets are 0.5 in in diameter and located at the right side of the fracture with a distance of 3 in in between. The mixed slurry was injected with a constant rate of 6 gpm and a concentration of 1.5 ppg. An outlet in the upper left corner allows the fluid and, thus the pressure to escape. Slickwater was used as fluid. For further details and parametrization, see Chun et al. (2020) and Table 2. Our numerical simulations adopt the same dimensions as in the experimental setup, except that our simulations are performed in 2D, and the aperture is used as a multiplication factor for the porosity and permeability in the solved equations as well as the inlet flow rates. If the maximum concentration (c = 0.62) is exceeded, which indicates a proppant bed built up in those elements, we change the slurry properties to pure water properties for modeling fluid flow in the porous proppant pack with updated porosity and permeability. The results are compared for two different timesteps (t = 10 s and t = 30 s) after the start of the injection.

Table 2: Parameter for the second benchmark case after Chun et al. (2020)

Parameter	**Unit**	**Value**
Fracture width	m	0.00762
Fracture length	m	1.2192
Fracture height	m	0.3048
Proppant diameter	m	0.000415
Proppant density	$kg.m^{-3}$	2550
Saturation concentration	-	0.62
Inlet proppant concentration	-	0.07
Inlet slurry rate	$m^3.s^{-1}$	0.000063
Carrying fluid density	$kg.m^{-3}$	1000
Carrying fluid viscosity	Pa.s	0.001
Outlet pressure	Pa	100000

Figure 3 presents the comparison of our results to the experimental data in Chun et al. (2020) and the simulation in Huang et al. (2022). The results show that settling is the main driving force for the movement of the dense particles in the low-viscosity carrying fluid. In the initial stage (t = 10 s) most of the particles settle in the first quarter of the entire fracture forming a growing immobile proppant bed (dark red color). Large parts of the fracture (and the outlet) are not covered by the proppant particles at all, which is shown as dark blue color.

At t = 30 s, a dune forms close to inlets clogging more than half of the fracture height. Close to the lower and middle inlet a zone of high advection velocities and strong internal mixing forms. This mixing zone is characterized by high contrasts in density/viscosity and can be well captured within the experiments as well as with our numerical model on the right-hand side of the fracture. The maximum height and slope of the propagating proppant bed cannot be perfectly tracked in our simulations due to the nature of the FE discretization and the necessary upwinding, which cause increased diffusive transport mainly close to the areas with saturation concentration. The fracture is mostly clogged by the settled proppant as observed from the experiment, while our simulations predict a maximum dune height of 2/3 of the fracture height. In contrast, the predicted maximum bedding length is increased as compared to the experimental results.

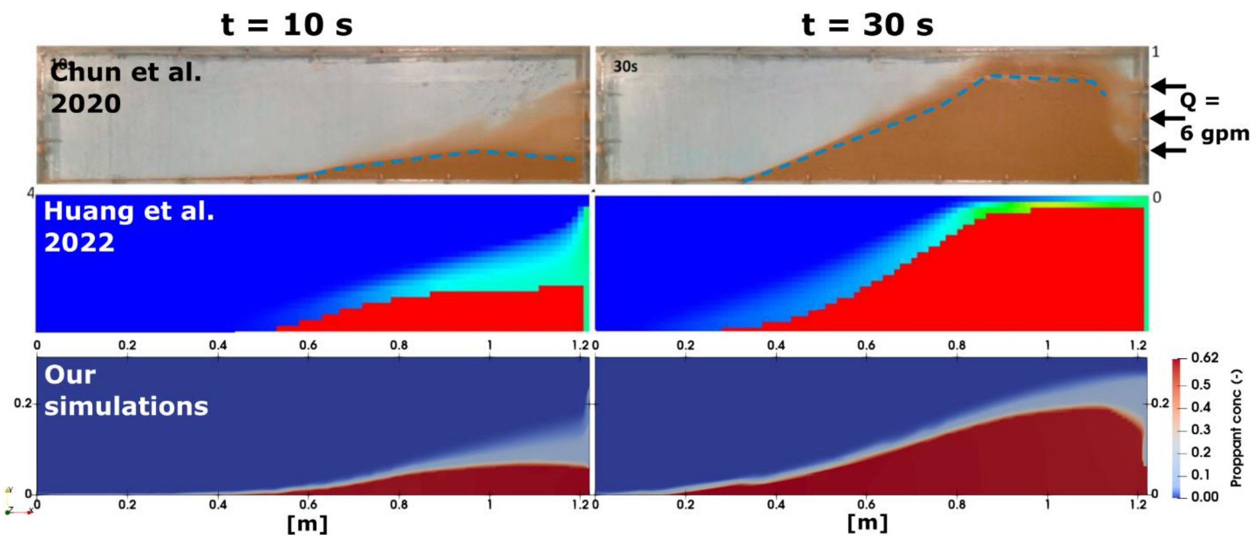

Figure 3: Comparison of our simulations to the experimental results of Chun et al. (2020) and the numerical model of Huang et al. (2022).

As described in the theory section as well as in Huang et al. (2022) and Detournay et al. (2016), the fluid flow in the proppant bed changes from fracture flow to porous media flow after proppant concentration reaches the maximum value (i.e., proppant saturation), as the proppant pack acting as immobile porous media. The density and viscosity of the flowing media changes to pure carrying fluid properties, while for the rest of the domain, those values are still determined by the constitutive equations in Section-2. Figure 4 shows density and viscosity as functions of the proppant concentration in the slurry. Dark red colors mark the regions close to the proppant bedding with high viscosity/density, while dark blue colors represent properties of the pure carrying fluid. In the vicinity of the immobile proppant bedding, a segregation zone that separates slurry flow and water flow occurs due to the high concentration and viscosity acting as hydraulic barrier with limited exchange and reduced vertical fluid migration.

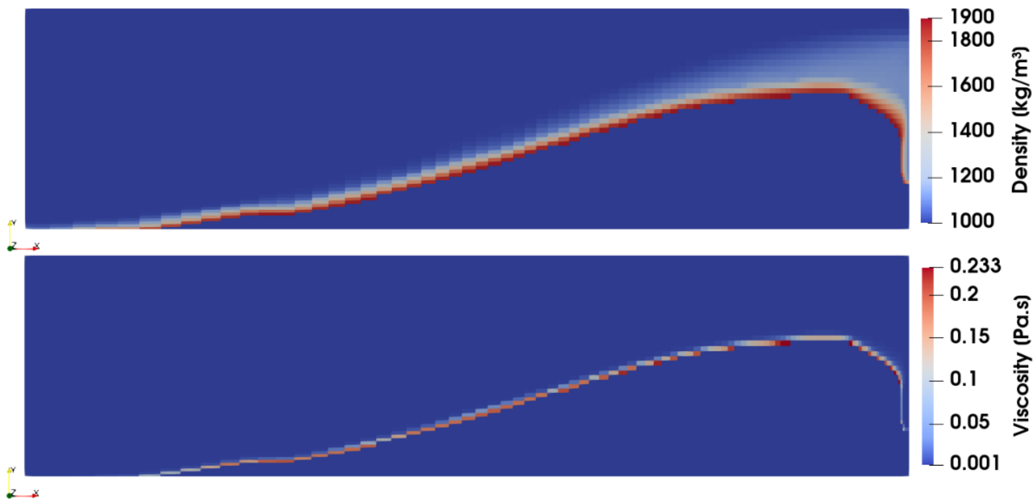

Figure 4: Density and viscosity of the slurry at the time of 30 s. High density/viscosity areas accumulate in the zones with concentrations close to the saturation.

3.3 Effects of fracturing fluid and proppant particles

The choice of slurry properties greatly affects the efficiency of hydraulic fracturing and the resulting fracture permeabilities. Therefore, we performed a sensitivity analysis with the simulated case at Section 3.2 as a base. We investigate the effects of the slurry rheology on the distribution of proppant particles by varying the proppant particle size and the viscosity of the fracturing fluid (Barboza et al., 2021). The proppant particle size affects the treatment for low-viscosity fluids, as coarse and high-density particles settle out rapidly and increase the risk of clogging the fracture. The selected particles (representing different kinds of fracture sands) and diameters (0.315 mm, 0.415 mm, 0.63 mm) reflect commonly used treatments (Huang et al., 2022). On the other hand, the viscosity of the fluid affects the overall process in two ways: one is the settling process (Eqs. 10-12) and the other is the velocity of the slurry (Eq. 16). Therefore, the simulated carrying fluid viscosities (0.1 mPa.s, 1 mPa.s and 10 mPa.s) reflect the usage of a gas-based fluid, slickwater and a linear gel. For all presented cases, a single vertical fracture is assumed, and the dimensions and injection scheme (regarding flow rates and inlet locations) are kept constant as described for the base case (Section 3.2).

Figure 5 shows the results of the sensitivity analysis, which compares proppant distribution at 30 s after injection for the base case (center) against the rest of the cases with changes in particle size (left) and fluid viscosity (right). It is clear that the particle diameter directly affects the settling velocity and, therefore, the settling location. Coarse particles immediately settle out of the low-viscosity slurry, resulting in a high dune near the inlet that extends almost the whole fracture height. Fine particles stay in suspension, which results in a flat proppant bed with a height less than half the fracture height. The increasing viscosity of the fluid affects the distribution of the proppant by changing the equilibrium height of the dune and slowing the settling of the particles from the slurry. The results indicate that a further decrease in viscosity (i.e., the case of μ=0.1 mPa.s) as compared to the base case has only a minor effect on the distribution of proppant and bedding. Immediate settling near the injection side dominates already for the low viscosity used in the base case. In contrast, an increase in viscosity is desirable for slurry transport. The particles settle uniformly along the entire length of the fracture, and we observe proppants are transported out of the domain as a residual concentration of proppant is predicted in the slurry close to the outlet.

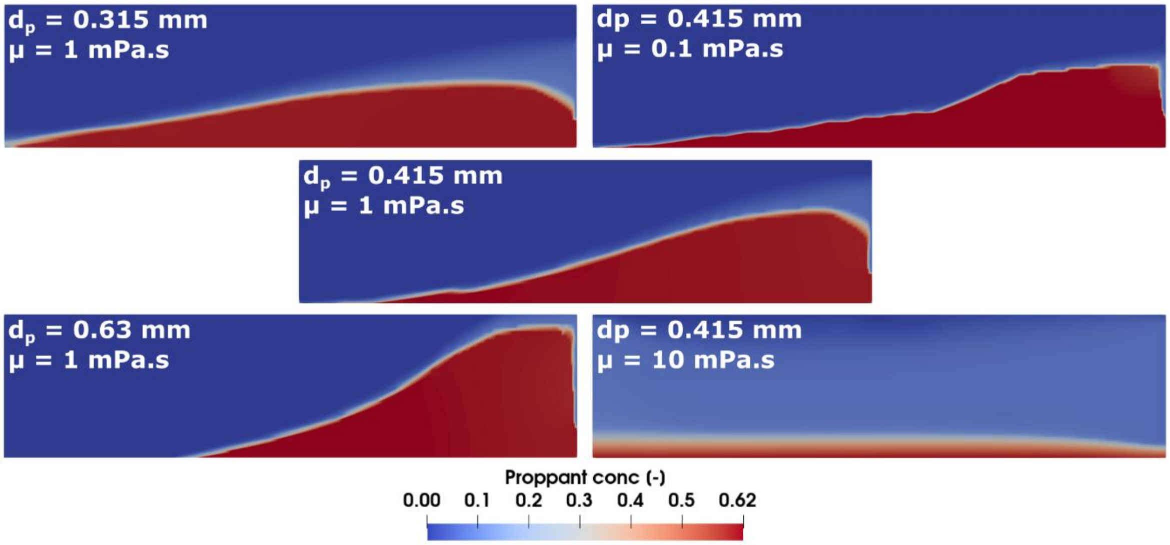

Figure 5: Sensitivity of the base case regarding changes in proppant particle size (left) and fluid viscosity (right). Dark red colors indicate maximum proppant saturation.

3.4 Hydraulic stimulation treatment

The previously shown examples reflect laboratory scale proppant injection scenarios assuming a constant fracture aperture in space and time. In the reservoir treatment, a newly created or existing fracture propagates into the matrix as a function of the injected fluid volume, pressure, and time. The slurry, injected during this treatment, follows the continuous increase in fracture length and width using the hydraulic gradient between the injection well and the fracture tip. Common hydraulic fracturing models are derived in literature, e.g. assuming KGD, PKN or penny-shaped fractures (Brady and Poe, 1992). The advantage of these fracturing models is the possibility to solve them semi-analytically as well as with 2D and 3D numerical models (Jin and Arson, 2019; Meng et al., 2023). Several parameters like the injected volume, rock physical properties and the fluid leak off into the matrix can be considered (Chen et al., 2021). In this section, we assume a penny-shaped fracture extending radially around an injection borehole and simulate the proppant distribution with ongoing fracture propagation and fluid injection.

Figure 6 shows the resulting aperture and proppant distribution of two individual timesteps (t = 1 s and 25 s) in a propagating disc-shaped fracture for a constant fluid injection 0.5 $kg.m^{-3}$. The parameters reflect the fracture width/length used in Peshcherenko and Chuprakov (2021), neglecting the leak off into the surrounding matrix and gravitational effects. A minimum aperture of $1x10^{-6}$ m is assumed in the unstimulated areas. The proppant particles and fluid rheology are assumed to be the same as the base case (Table 2), except the injected slurry has a proppant concentration of 5 %. In the first few seconds, the slurry lacks behind the fracture extension resulting in less concentration at the fracture tips. With ongoing treatment, the slurry accumulates in the fracture tip and areas with less aperture.

Note that in this simplified example, gravitational effects such as a hydrostatic pressure gradient and settling of particles were not considered. Those effects would result in a non-ideal radial fracture and accumulation of proppant particles at the bottom of the fracture. However, comparison with analytical solutions is then no longer possible and the mutual coupling of all physical processes is required. In addition, closure effects, such as decreasing apertures and backflow of proppant, will be considered in a future study.

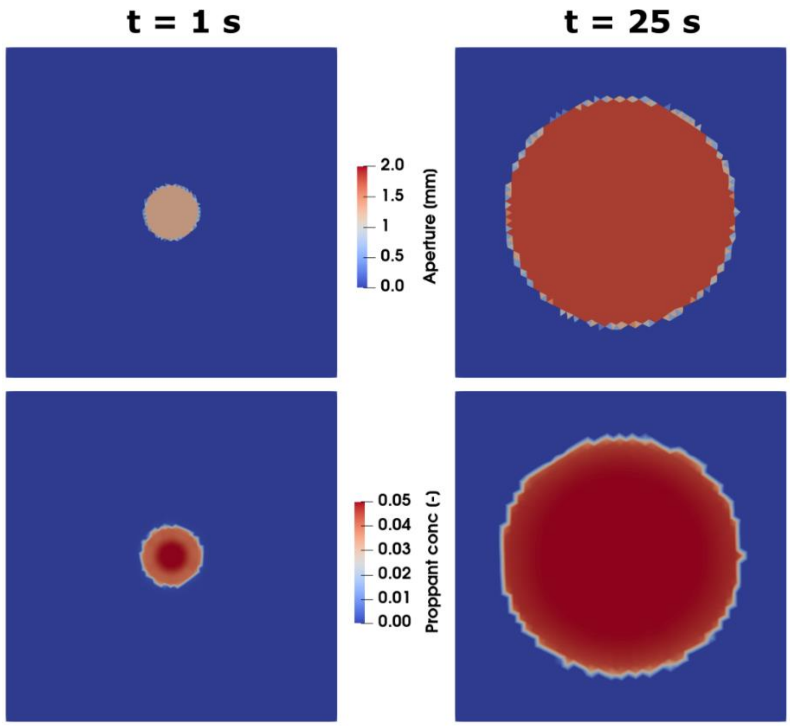

Figure 6: Simultaneous injection of slurry with fracturing treatment into a radial extending fracture. The fracture length/width extends with time, and the slurry follows the newly generated fracture void space.

4. Conclusion

We have developed a workflow to simulate the transportation of proppant particles during hydraulic fracturing. This study focuses on the implementation and validation of the physical processes associated with the transport of a particle-laden slurry. The slurry is a mixture of a low-viscosity fracturing fluid and high-density proppant particles. Processes involved include advective transport in the mixture, settling on the bottom of the fracture, hindered settling due to particle-particle interactions, and the change of the flow system from fracture to porous media flow with increasing proppant concentrations.

The workflow is developed in the multiphysical MOOSE framework. Our model is benchmarked against different experimental (Chun et al., 2020; Tong and Mohanty, 2016) and numerical simulations (Hu et al., 2018; Huang et al., 2022). In addition, we demonstrated the ability of the modeling workflow to account for different fluid rheologies, concentration-dependent properties, proppant particles and injection schemes. The parameters used reflect the most common fracturing fluids and proppant particles in the context of a hydraulic fracturing treatment. Furthermore, the effect of leak-off into permeable host rocks or partially filled fractures can be considered. Due to the modular structure of the MOOSE framework, each physical process can be evaluated and treated individually. Finally, we presented preliminary results of a combined simulation of hydraulic fracturing with simultaneous slurry transport. The workflow targets the improvement of the hydraulic fracturing design. It helps to predict and optimize the stimulation treatment and to translate laboratory experimental results into field operation guidelines. In the future, the model will be extended to capture further mechanical processes involved in the treatment, like fracture tip behavior, fracture closure, and associated proppant bridging.

Acknowledgement

The information, data, or work presented herein was funded in part by the Advanced Research Projects Agency-Energy (ARPA-E), U.S. Department of Energy (DOE), under Award Number DE-AR0001709. Any opinions, findings and conclusions, or recommendations expressed in this material are those of the authors and do not necessarily reflect those of the DOE or the U.S. Government. This research made use of Idaho National Laboratory computing resources which are supported by the Office of Nuclear Energy of the U.S. DOE and the Nuclear Science User Facilities under Contract No. DE-AC07-05ID14517.

REFERENCES

Adachi, J., Siebrits, E., Peirce, A., and Desroches, J. "Computer simulation of hydraulic fractures." *International Journal of Rock Mechanics and Mining Sciences*, 44, 5, (2007), 739-757.

Barboza, B. R., Chen, B., and Li, C. "A review on proppant transport modelling." *Journal of Petroleum Science and Engineering*, 204, (2021).

Barree, R. D., and Conway, M. W. "Experimental and Numerical Modeling of Convective Proppant Transport." *Journal of Petroleum Technology*, 47, 03, (1995), 216-222.

Brady, B., and Poe, B. "Cracking rock: Progress in Fracture Treatment Design." *Oilfield Review*, (1992).

Carman, P. C. "Fluid flow through granular beds." *Trans Inst Chem Eng* 15, (1937), 150–166.

Chen, B., Barboza, B. R., Sun, Y., Bai, J., Thomas, H. R., Dutko, M., Cottrell, M., and Li, C. "A Review of Hydraulic Fracturing Simulation." *Archives of Computational Methods in Engineering*, 29, 4, (2021), 1-58.

Chun, T., Li, Y., and Wu, K. "Comprehensive experimental study of proppant transport in an inclined fracture." *Journal of Petroleum Science and Engineering*, 184, (2020).

Clark, P. E., and Quadir, J. A. "Prop Transport In Hydraulic Fractures: A Critical Review Of Particle Settling Velocity Equations." *Proceedings: SPE/DOE Low Permeability Gas Reservoirs Symposium*, Denver, (1981).

Detournay, C., Lemos, J., and Zhang, F. "Development of a proppant transport logic in 3DEC." *in* Gomez, P., ed., Applied numerical modeling in geomechanics, (2016).

Egert, R., Gholami Korzani, M., Held, S., and Kohl, T. "Implications on large-scale flow of the fractured EGS reservoir Soultz inferred from hydraulic data and tracer experiments." *Geothermics*, 84, (2020).

Gadde, P. B., Liu, Y., Norman, J., Bonnecaze, R., and Sharma, M. M. "Modeling Proppant Settling in Water-Fracs." *Proceedings: SPE Annual Technical Conference and Exhibition*, Houston, (2004).

Hu, X., Wu, K., Song, X., Yu, W., Tang, J., Li, G., and Shen, Z. "A new model for simulating particle transport in a low-viscosity fluid for fluid-driven fracturing." *AIChE Journal*, 64, 9, (2018), 3542-3552.

Huang, J., Hao, Y., Settgast, R. R., White, J. A., Mateen, K., and Gross, H. "Validation and Application of a Three-Dimensional Model for Simulating Proppant Transport and Fracture Conductivity." *Rock Mechanics and Rock Engineering*, (2022).

Isah, A., Hiba, M., Al-Azani, K., Aljawad, M. S., and Mahmoud, M. "A comprehensive review of proppant transport in fractured reservoirs: Experimental, numerical, and field aspects." *Journal of Natural Gas Science and Engineering*, 88, (2021).

Jin, W., and Arson, C. "Fluid-driven transition from damage to fracture in anisotropic porous media: a multi-scale XFEM approach." *Acta Geotechnica*, 15, 1, (2019), 113-144.

Kumar, D., Gonzales, R., and Ghassemi, A. "The Role of Micro-Proppants in Conductive Fracture Network Development." *Proceedings: SPE Hydraulic Fracturing Technology Conference and Exhibition*, The Woodlands, (2019).

Lindsay, A. D., Gaston, D. R., Permann, C. J., Miller, J. M., Andrs, D., Slaughter, A. E., Kong, F. D., Hansel, J., Carlsen, R. W., Icenhour, C., Harbour, L., Giudicelli, G. L., Stogner, R. H., German, P., Badger, J., Biswas, S., Chapuis, L., Green, C., Hales, J., Hu, T. C., Jiang, W., Jung, Y. S., Matthews, C., Miao, Y. B., Novak, A., Peterson, J. W., Prince, Z. M., Rovinelli, A., Schunert, S., Schwen, D., Spencer, B. W., Veeraraghavan, S., Recuero, A., Yushu, D., Wang, Y. Q., Wilkins, A., and Wong, C. S. P. "2.0-MOOSE: Enabling massively parallel multiphysics simulation." *Softwarex*, 20, (2022).

Meng, C., Fournier, A., and Jin, W. "A Split-node Method for Modeling Pulse and Hydraulic Fracturing." *Proceedings: ARMA Symposium*, Atlanta, (2023).

Nicodemo, L., Nicolais, L., and Landel, R. F. "Shear rate dependent viscosity of suspensions in newtonian and non-newtonian liquids." *Chemical Engineering Science*, 29, 3, (1974), 729-735.

Peshcherenko, A., and Chuprakov, D. "An ultrafast simulator for 3D propagation of a hydraulic fracture with rectangular shape." *Engineering Fracture Mechanics*, 243, (2021).

Schill, E., Genter, A., Cuenot, N., and Kohl, T. "Hydraulic performance history at the Soultz EGS reservoirs from stimulation and long-term circulation tests." *Geothermics*, 70, (2017), 110-124.

Shiozawa, S., and McClure, M. "Simulation of proppant transport with gravitational settling and fracture closure in a three-dimensional hydraulic fracturing simulator." *Journal of Petroleum Science and Engineering*, 138, (2016), 298-314.

Shook, C. A., and Roco, M. C. "Slurry flow - principles and practice." Butterworth, (1991).

Tong, S., and Mohanty, K. K. "Proppant transport study in fractures with intersections." *Fuel*, 181, (2016), 463-477.

Wang, J., and Elsworth, D. "Role of proppant distribution on the evolution of hydraulic fracture conductivity." *Journal of Petroleum Science and Engineering*, 166, (2018), 249-262.

Wang, J., Joseph, D. D., Patankar, N. A., Conway, M., and Barree, R. D. "Bi-power law correlations for sediment transport in pressure driven channel flows." *International Journal of Multiphase Flow*, 29, 3, (2003), 475-494.

Wilkins, A., Green, C. P., and Ennis-King, J. "An open-source multiphysics simulation code for coupled problems in porous media." *Computers & Geosciences*, 154, (2021).